Supporting Information

Exploring the Role of Peptide Helical Stability in the Propensity of Uperin 3.*x* Peptides toward Beta-Aggregation

Sourav Ray[†, §, ‡], Stephanie Holden[§], Anup Kumar Prasad[†, §, ‡],

Lisandra L Martin[§], and Ajay Singh Panwar[‡]

[†]IITB-Monash Research Academy, Indian Institute of Technology Bombay, Powai, Mumbai–400076, India

[§]School of Chemistry, Monash University, Clayton 3800, Victoria, Australia

[‡]Department of Metallurgical Engineering and Materials Science, Indian Institute of Technology Bombay, Powai, Mumbai–400076, India

S1. α-helix-to-coil transition

As the simulations of the six U3*.x* (wt and R/K7A) peptides proceed, all with α-helical starting structures, the helical content of the peptides gradually decreases as observed in Figure S1. However, a short-lived increase in helical content was observed in some of the simulations after the initial transition. Negligible β-content could be observed over the entire simulation period in Figure S2. The turn secondary structure content remained at a certain level as shown in Figure S3. Increase in coil content in Figure S4 is commensurate with the decrease in helical content over the 800 ns simulation period.

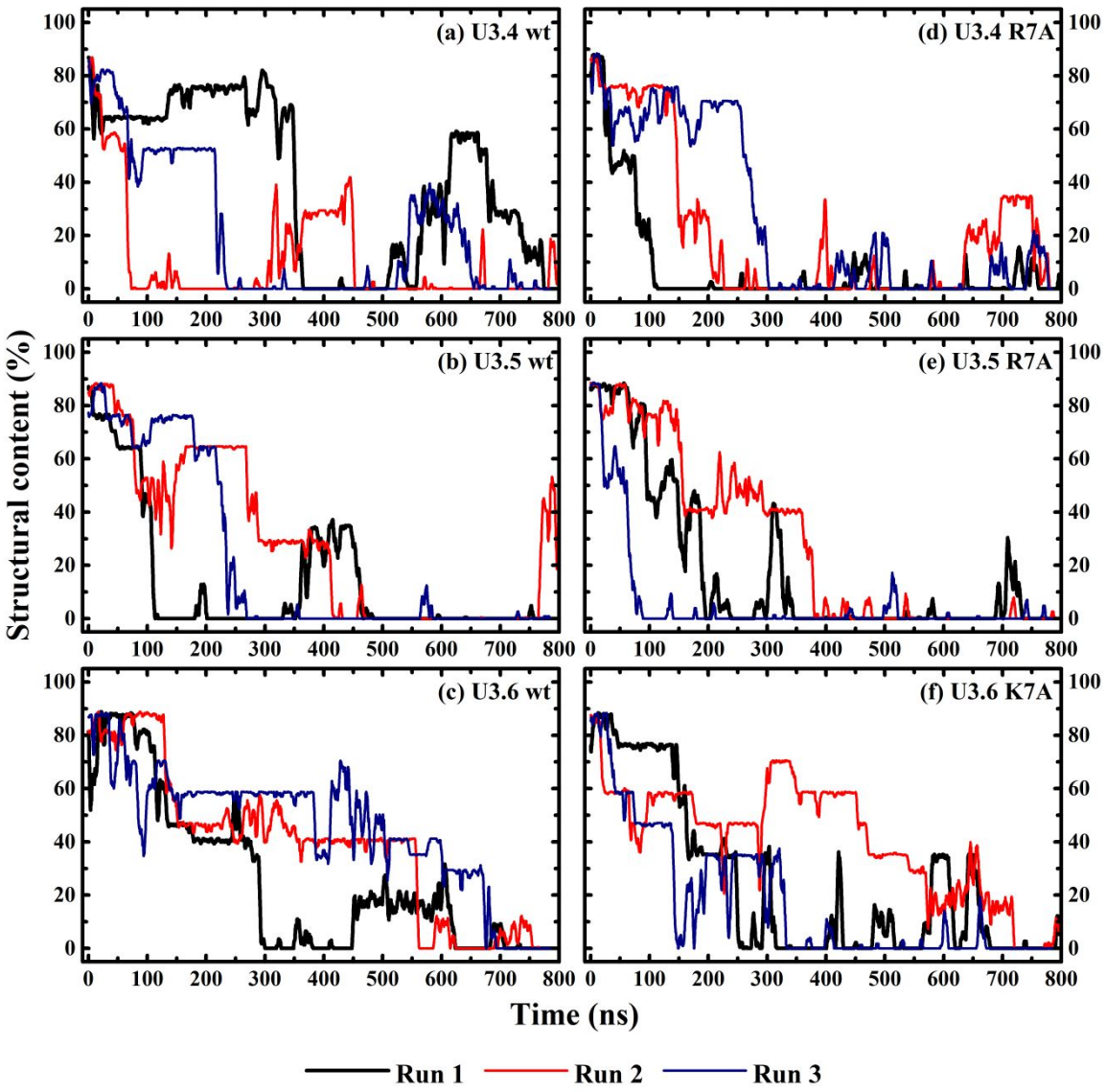

Figure S1. Helical secondary structure content variation in different runs of (a) U3.4 wt, (b) U3.5 wt and (c) U3.6 wt peptides, and corresponding (d) U3.4 R7A, (e) U3.5 R7A and (f) U3.6 K7A variants, over the simulation time periods.

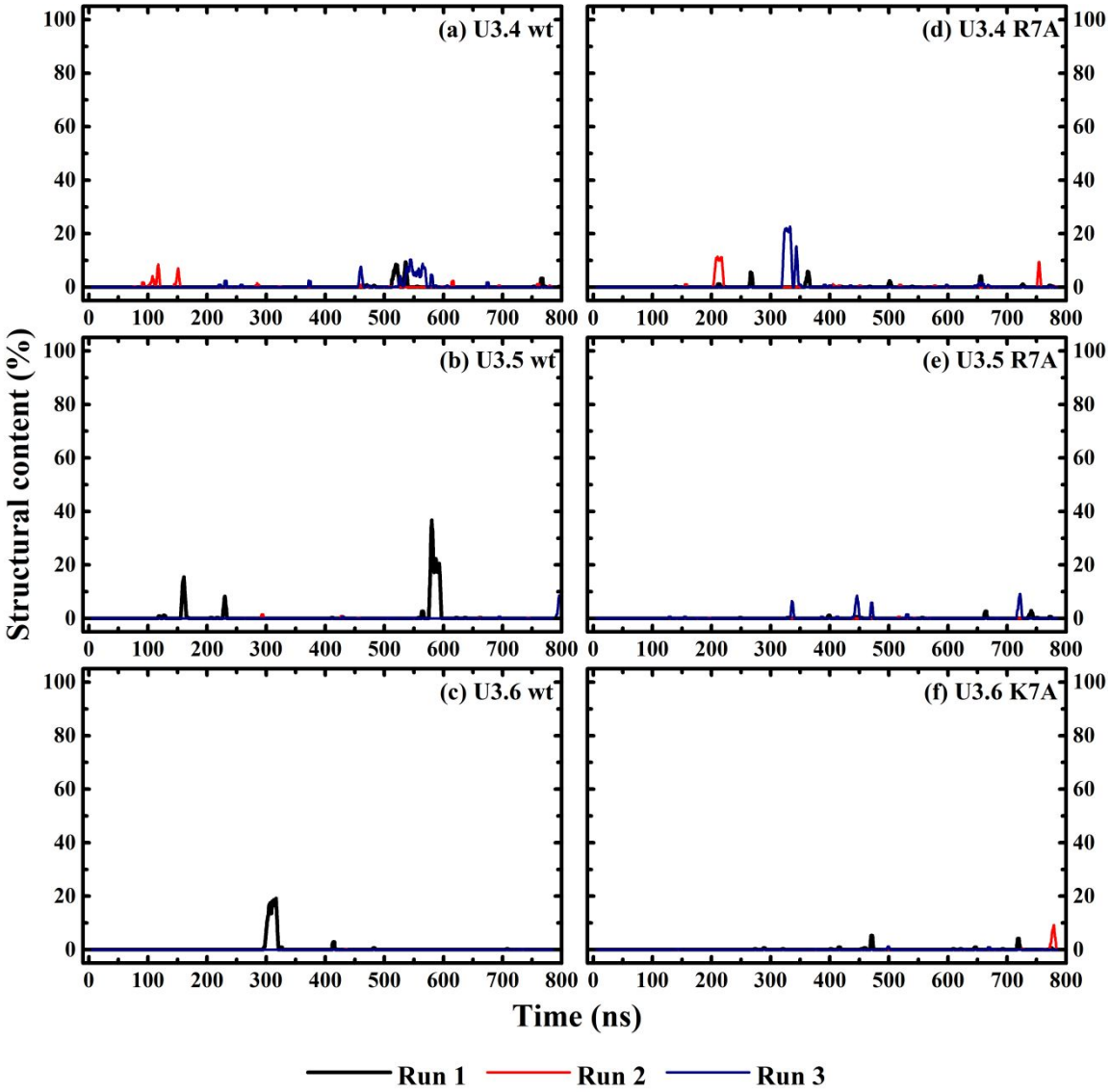

Figure S2. Beta secondary structure content variation in different runs of (a) U3.4 wt, (b) U3.5 wt and (c) U3.6 wt peptides, and corresponding (d) U3.4 R7A, (e) U3.5 R7A and (f) U3.6 K7A variants, over the simulation time periods.

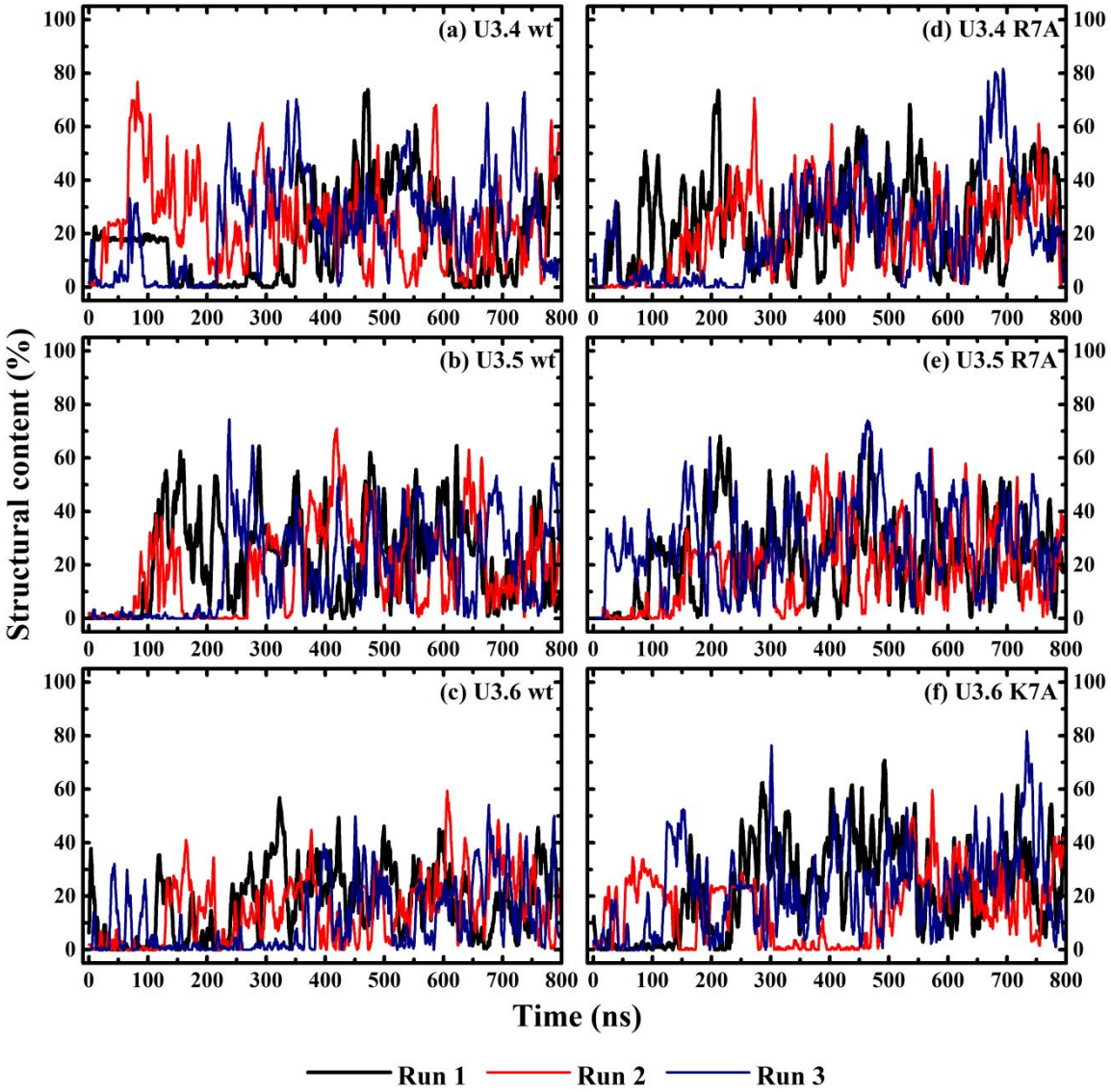

Figure S3. Turn secondary structure content variation in different runs of (a) U3.4 wt, (b) U3.5 wt and (c) U3.6 wt peptides, and corresponding (d) U3.4 R7A, (e) U3.5 R7A and (f) U3.6 K7A variants, over the simulation time periods.

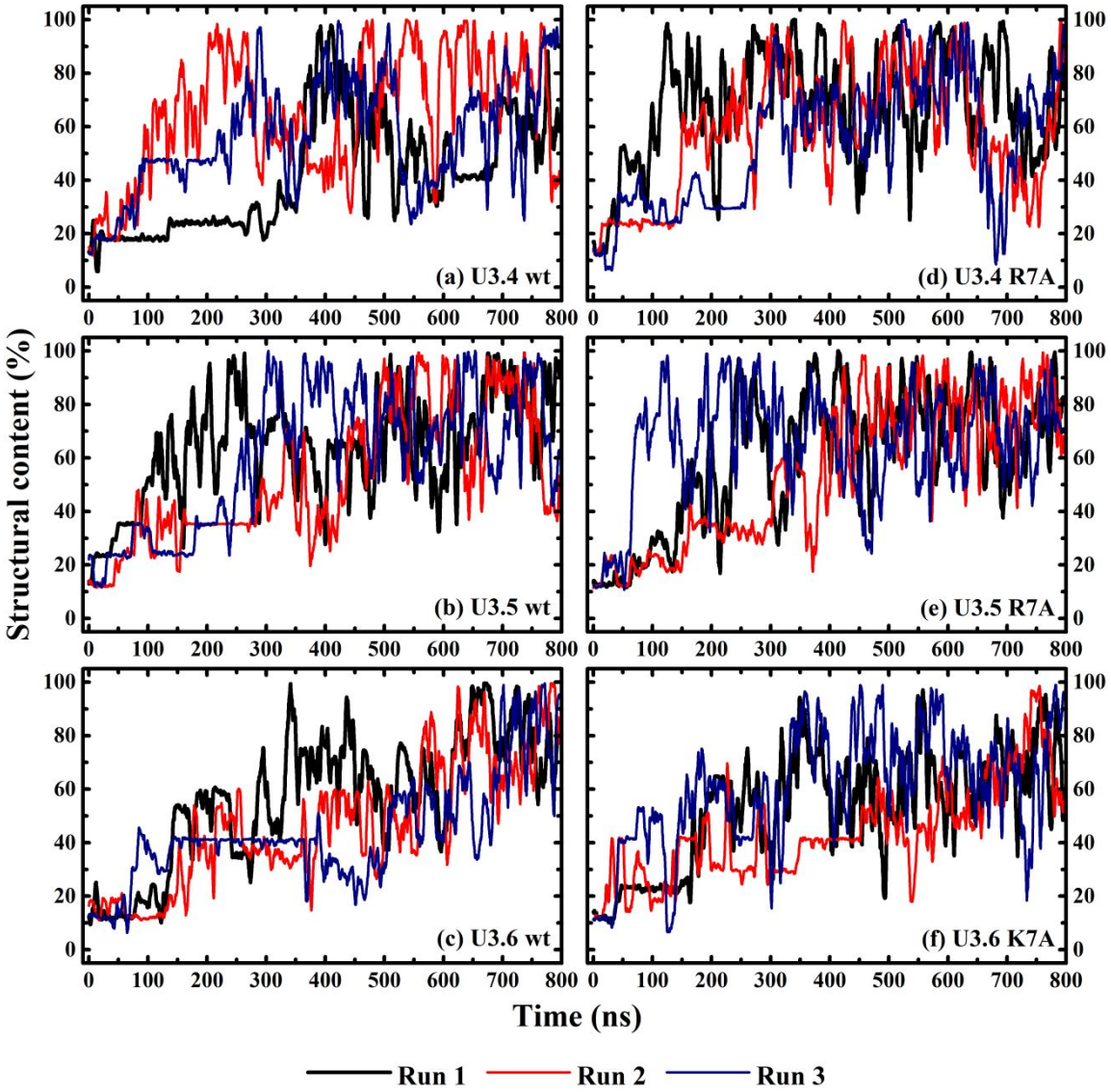

Figure S4. Coil secondary structure content variation in different runs of (a) U3.4 wt, (b) U3.5 wt and (c) U3.6 wt peptides, and corresponding (d) U3.4 R7A, (e) U3.5 R7A and (f) U3.6 K7A variants, over the simulation time periods.

S2. Docking and propagation

After self-docking the centroid peptide conformers using the Hex program[S1], docking energy values were obtained. It should be noted that these unitless energy values are from a reference energy point where the peptides are at a supposedly infinite separation or zero interaction, and negative scores represent a favourable docking[S2]. Although these values are irrelevant on an absolute scale, but they provide a relative measure of docking favourability. After Hex docking, search for propagating conformers was carried out with an intermediate post-processing step of OPLS energy minimisation[S3]. The propagating conformers for each of the six U3.*x* (wt and R/K7A) peptides are listed in Table S1.

Table S1. Hex docking energies and secondary structure composition of propagating conformers of (a) U3.4 wt, (b) U3.5 wt, (c) U3.6 wt, (d) U3.4 R7A, (e) U3.5 R7A and (f) U3.6 K7A.

Conformer Family (CF)	Docking energy	Secondary structure composition
(a) U3.4 wt		
15*	-289.56	Turn, Coil
16	-252.77	Turn, Coil
(b) U3.5 wt		
11*	-294.38	Turn, Coil
19	-229.01	Turn, Coil
(c) U3.6 wt		
06	-244.91	α-helix, turn, coil
07	-255.04	α-helix, coil
11	-287.41	Isolated β-bridge, coil
17*	-311.59	Turn, coil
19	-278.43	3_{10}-helix, turn, coil
(d) U3.4 R7A		
04	-257.50	α-helix, turn, coil
08	-261.32	α-helix, turn, coil
14*	-260.88	Coil
(e) U3.5 R7A		
01	-225.75	α-helix, coil
03	-296.28	α-helix, turn, coil
04	-296.82	α-helix, turn, coil
09	-342.35	Turn, Coil
13	-276.75	α-helix, isolated β-bridge, turn, coil
15	-308.53	Turn, Coil
17	-323.68	α-helix, turn, coil
21*	-409.36	Turn, Coil
(f) U3.6 K7A		
21*	-257.29	Isolated β-bridge, turn, coil

*Propagating conformer selected for further analyses in Figures 8–12.

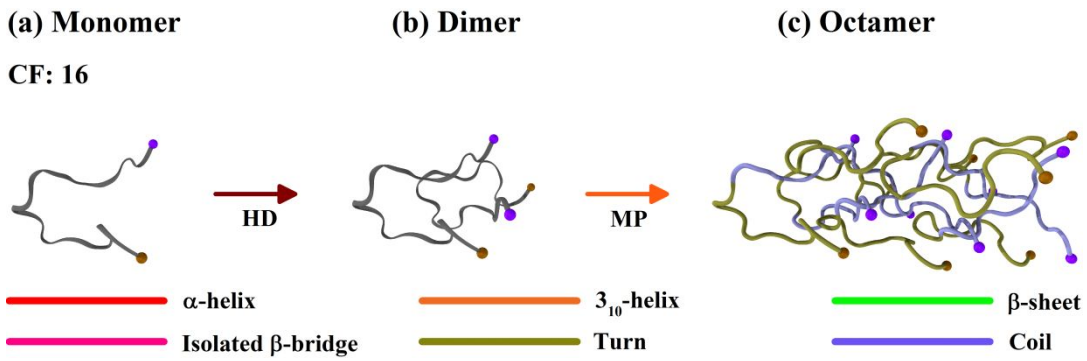

Figure S5. (a) Propagating conformers of U3.4 wt, (b) self-docked using Hex. (c) Transformation matrix used to generate an octamer aggregate.

For U3.4 wt propagating conformers in Table S1a, the CF: 15 conformer has the lowest Hex docking energy for dimers. Therefore, it was selected for further analysis. HD and MP denote Hex Docking and Matrix Propagation, respectively.

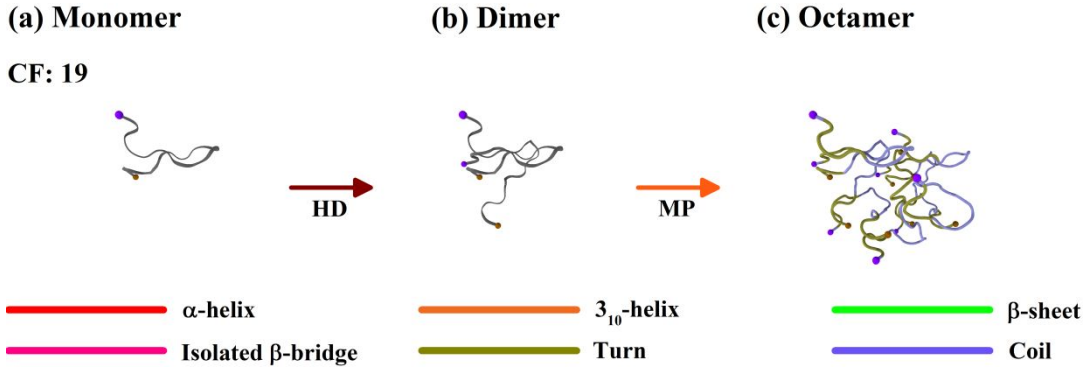

Figure S6. (a) Propagating conformers of U3.5 wt, (b) self-docked using Hex. (c) Transformation matrix used to generate an octamer aggregate.

In case of U3.5 wt octamers in Table S1b, the CF: 11 octamer was selected since it has a more favourable Hex docking energy for dimers.

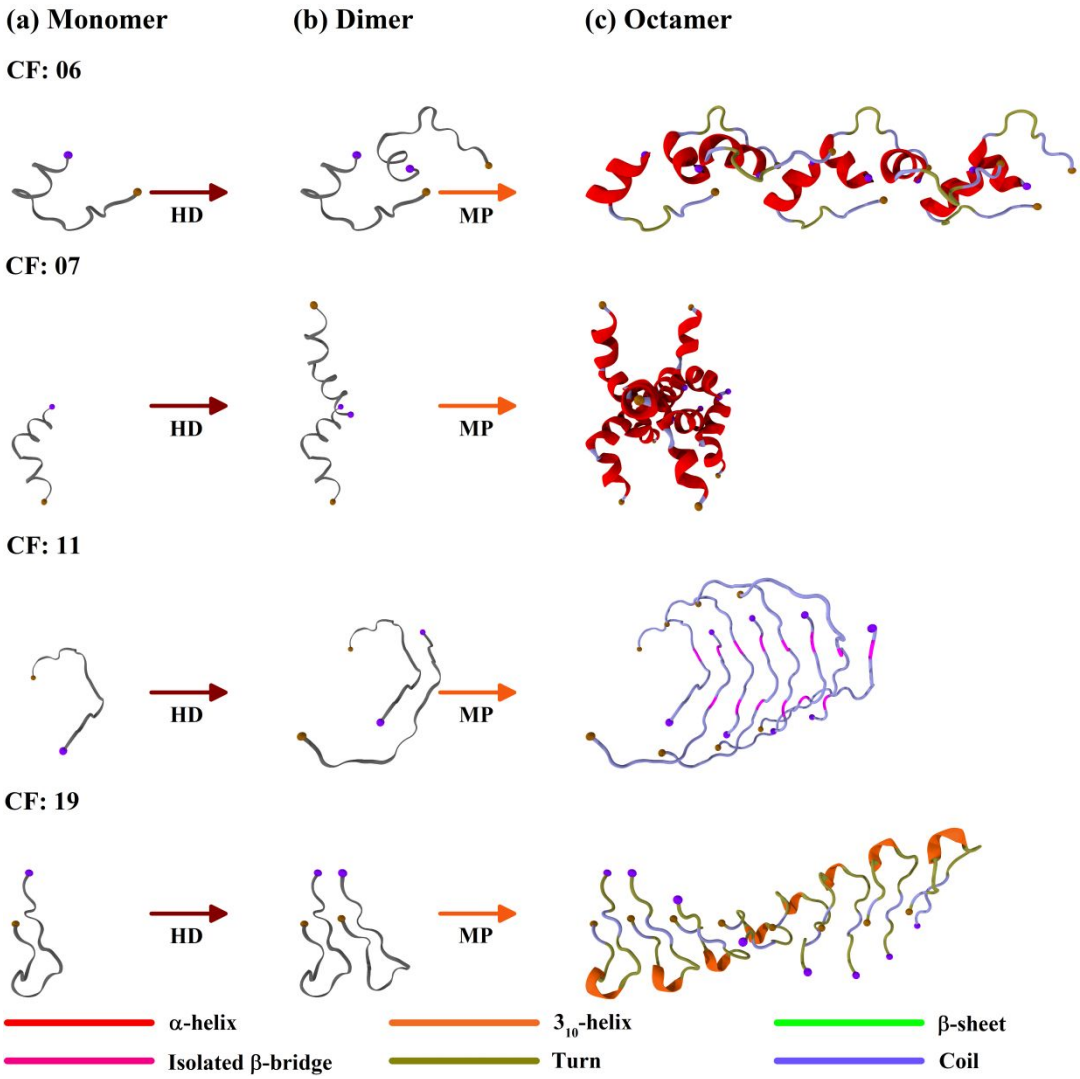

Figure S7. (a) Propagating conformers of U3.6 wt, (b) self-docked using Hex. (c) Transformation matrix used to generate an octamer aggregate.

The CF: 17 octamer of U3.6 wt was selected for analysis, as it had the next most favourable docking energy for dimers, as noted in Table S1c.

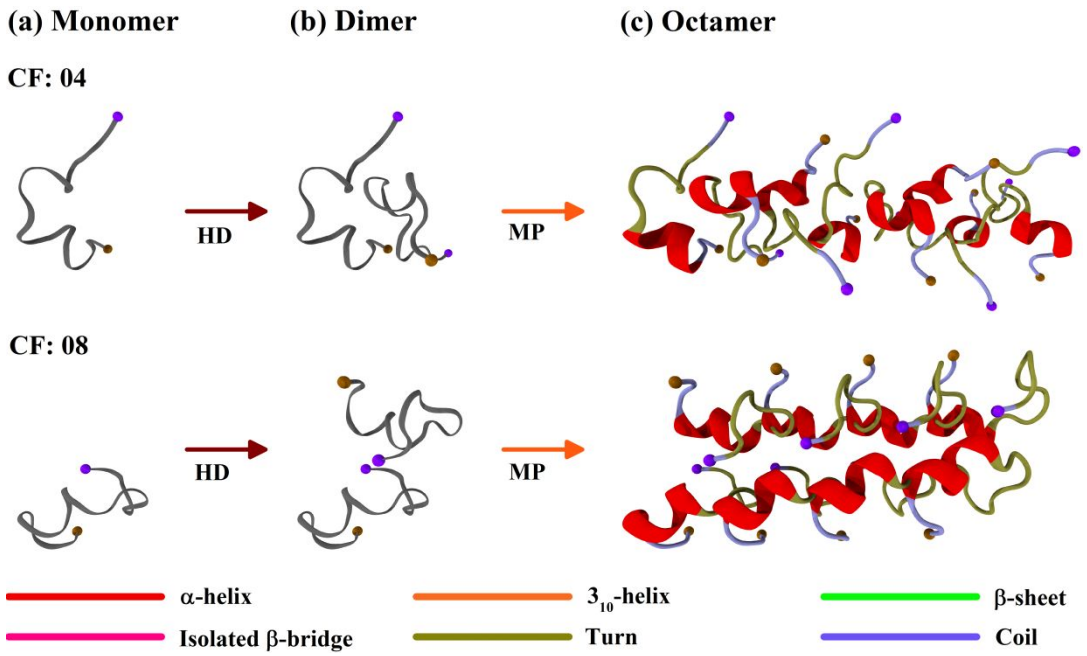

Figure S8. (a) Propagating conformers of U3.4 R7A, (b) self-docked using Hex. (c) Transformation matrix used to generate an octamer aggregate.

For propagating conformers of U3.4 R7A in Table S1d, the CF: 08 octamer has appreciable α-helical content, and therefore this octamer was not considered (reason explained in detail in the discussion for Figure S11). The CF: 14 octamer, whose Hex docking energy for dimers is very similar to that of CF: 08 octamer, was chosen for further analysis.

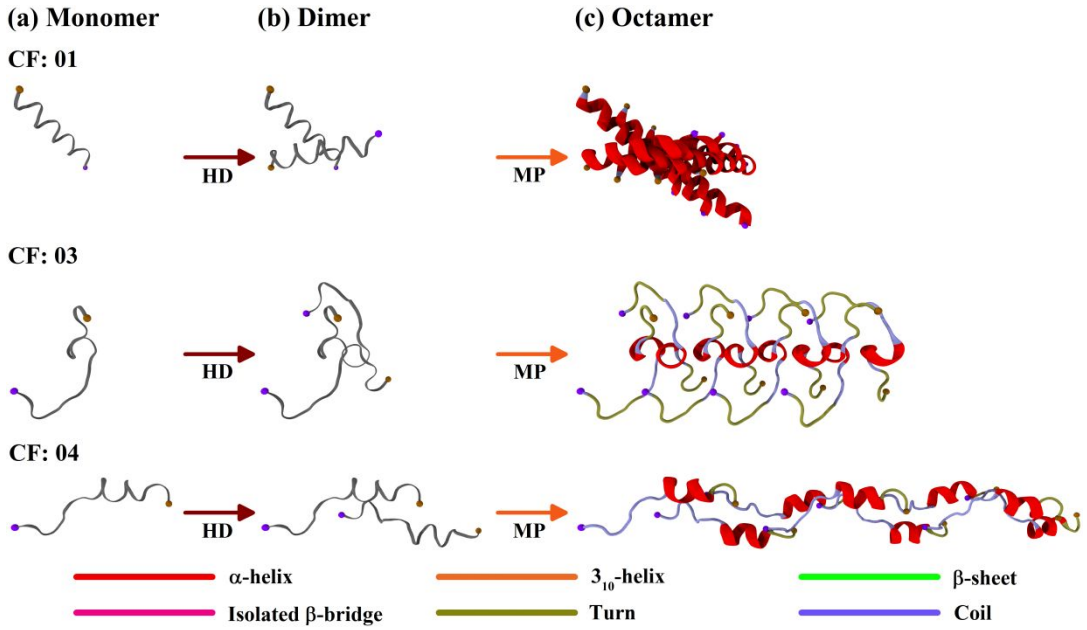

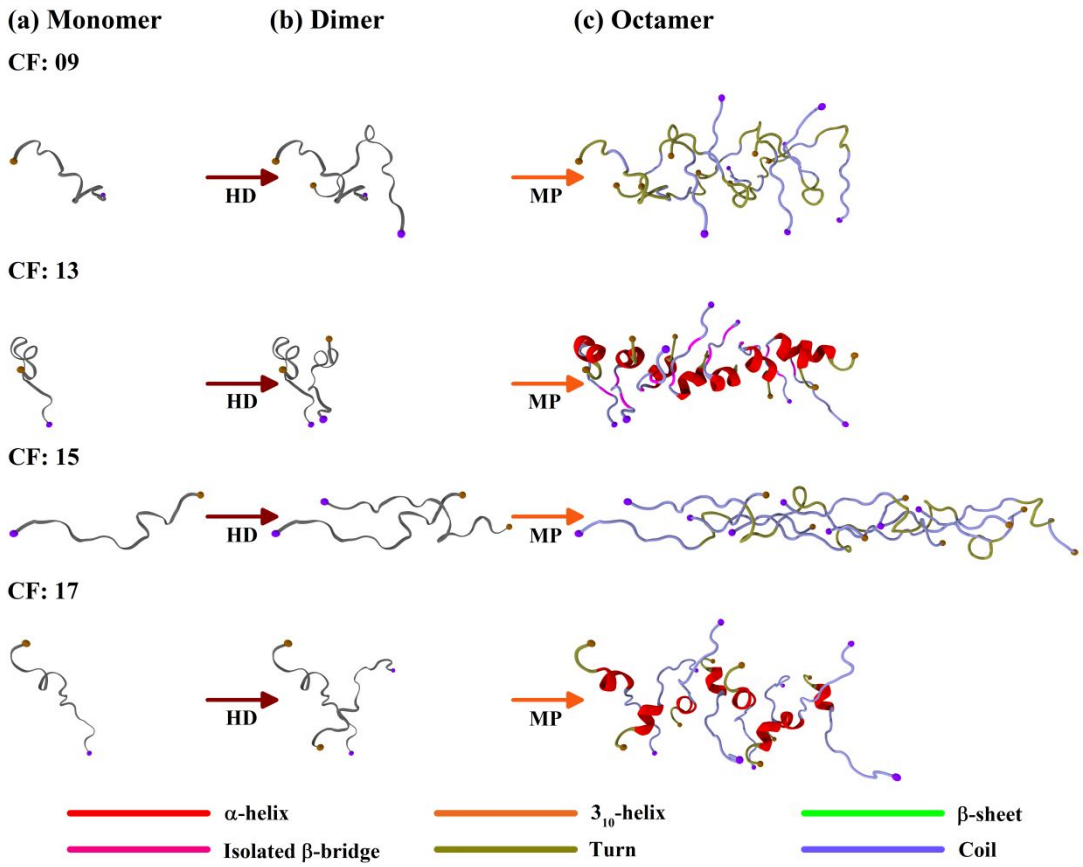

Figure S9. (a) Propagating conformers of U3.5 R7A, (b) self-docked using Hex. (c) Transformation matrix used to generate an octamer aggregate.

In case of U3.5 R7A conformers in Table S1e, the CF: 21 has the most favourable Hex docking energy for dimers. Hence, the CF: 21 octamer was picked for further analysis.

Only one propagating conformer was obtained for U3.6 K7A, as observed in Table S1f, and therefore the CF: 21 octamer was selected for further analysis.

S3. Octamer analysis

For most of the uperin 3.x peptides and variants, multiple octamers were simulated to track their stability and secondary structure evolution over the 100 ns simulation period. As discussed in Figure 7, the seventh position alanine variant octamers selected for detailed analysis remained more stable during the simulations, compared to the corresponding wild-type octamers in Figure S10.

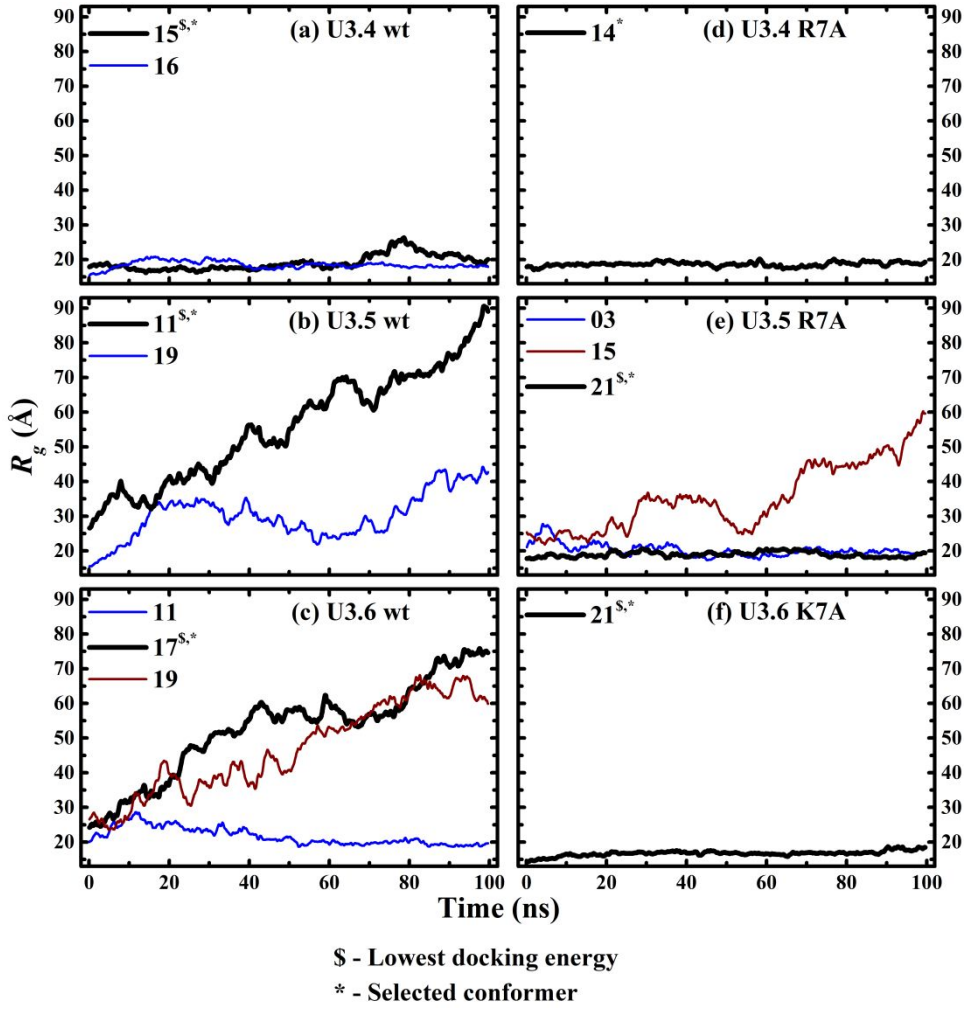

Figure S10. R_g plots of some of the octamers of (a) U3.4 wt, (b) U3.5 wt, (c) U3.6 wt, (d) U3.4 R7A, (e) U3.5 R7A and (f) U3.6 K7A, over the entire simulation period.

The variant octamers selected for detailed analysis demonstrated a higher β-sheet content than the corresponding wild-type octamers in Figure S11, a trend also noted in Figure 9a. Furthermore, octamers with an appreciable α-helical content at the onset were found to display slower transition to β-sheet structures than ones with exclusively turn and coil secondary structure content. This could be clearly noted for the U3.5 R7A octamers of CF: 03 and CF: 21 conformers in Table S1e and Figure S11e. The overall β-sheet content for the CF: 03 octamer reached only 12% towards the end of the simulation, compared to the 20% observed for the CF: 21 octamer. Hence, the transition to β-sheet content observed for the CF: 03 octamer is significantly slower than that observed for the CF: 21 octamer of U3.5 R7A. Therefore, as noted previously in Figure 6c and Table S1, the selected octamers of all U3.*x* peptides and variants predominantly consist of turn and coil secondary structure elements. However,

intermediate conformers with α-helical signatures might play a crucial role in amyloid fibril formation[S4].

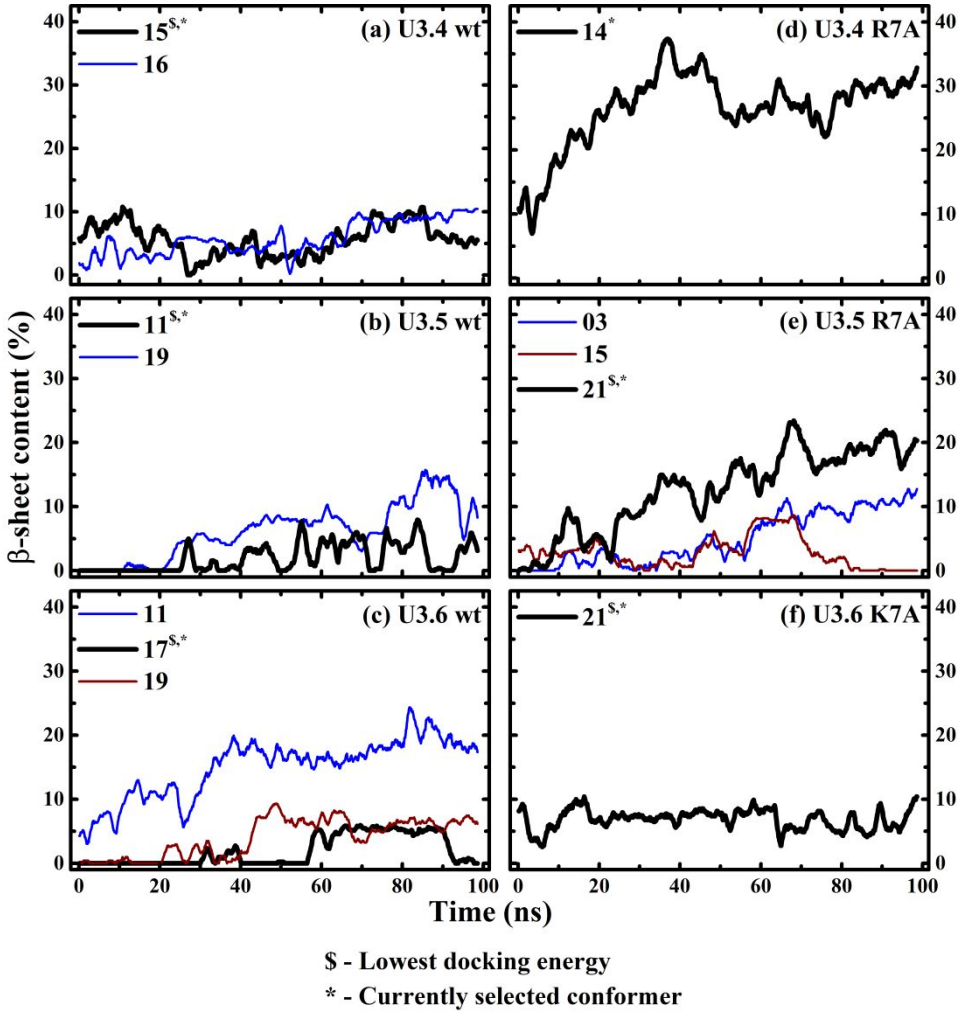

Figure S11. The evolution of β-sheet content over the entire simulation period of some of the octamers of (a) U3.4 wt, (b) U3.5 wt, (c) U3.6 wt, (d) U3.4 R7A, (e) U3.5 R7A and (f) U3.6 K7A.

S4. Intrinsic residue solubility profiles

Greater aggregation in the N-terminal region of U3.*x* R/K7A variants, relative to the U3.*x* wild-type peptides, can be observed in the intrinsic residue solubility profiles, as calculated using the CamSol method[S5-S7]. A score is assigned to each residue of the peptide sequence, with residues having a score greater than 1 being highly soluble, and those with a score lower than -1 being poorly soluble in aqueous environments. Higher solubility indicates lower aggregation propensity, and vice versa. As illustrated in Figure S12, where cationic to hydrophobic residue

substitution occurs (position 7), a clear decrease in the solubility of the U3*.x* R/K7A peptides is observed relative to the U3*.x* wild-type peptides in this study.

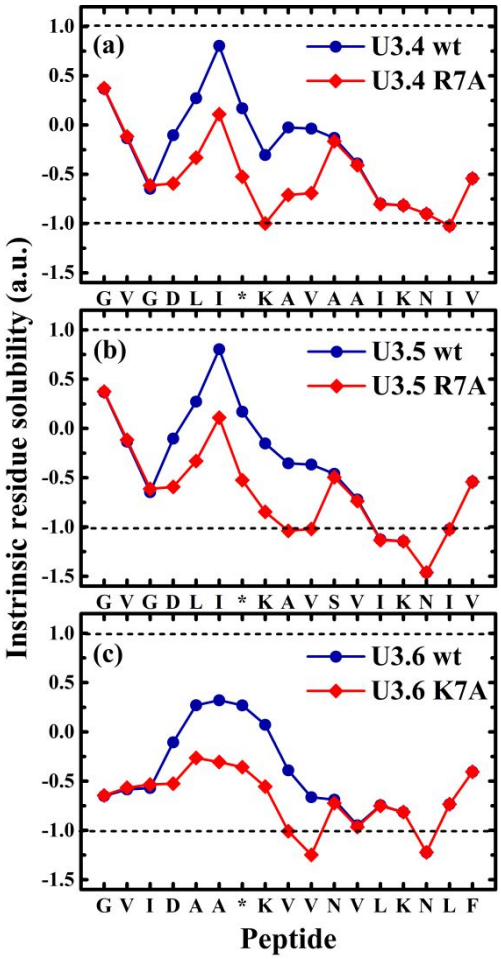

Figure S12. Intrinsic residue solubility profiles of (a) U3.4 wt and R7A, (b) U3.5 wt and R7A, and (c) U3.6 wt and K7A peptides calculated using the Camsol method[S5-S6].

S5. References

S1. Macindoe, G.; Mavridis, L.; Venkatraman, V.; Devignes, M.-D.; Ritchie, D. W., Hexserver: An Fft-Based Protein Docking Server Powered by Graphics Processors. *Nucleic Acids Research* **2010**, *38*, W445-W449.

S2. Ritchie, D. W., Hex 8.0.0 User Manual. *INRIA Nancy Grand Est, LORIA c) https://members.loria.fr/DRitchie/* **2013**.

S3. Ritchie, D. W., Evaluation of Protein Docking Predictions Using Hex 3.1 in Capri Rounds 1 and 2. *Proteins: Structure, Function, and Bioinformatics* **2003**, *52*, 98-106.

S4. Lin, Y.-S.; Pande, V. S., Effects of Familial Mutations on the Monomer Structure of Aβ42. *Biophysical Journal* **2012**, *103*, L47-L49.

S5. Sormanni, P.; Amery, L.; Ekizoglou, S.; Vendruscolo, M.; Popovic, B., Rapid and Accurate in Silico Solubility Screening of a Monoclonal Antibody Library. *Scientific Reports* **2017**, *7*, 8200.

S6. Sormanni, P.; Aprile, F. A.; Vendruscolo, M., The Camsol Method of Rational Design of Protein Mutants with Enhanced Solubility. *Journal of Molecular Biology* **2015**, *427*, 478-490.

S7. Martin, L. L.; Kubeil, C.; Piantavigna, S.; Tikkoo, T.; Gray, N. P.; John, T.; Calabrese, A. N.; Liu, Y.; Hong, Y.; Hossain, M. A., Amyloid Aggregation and Membrane Activity of the Antimicrobial Peptide Uperin 3.5. *Pept. Sci.* **2018**, *e24052*.